ATP Inhibition and Rectification of a Ca^{2+}-Activated Anion Channel in Sarcoplasmic Reticulum of Skeletal Muscle

Gerard P. Ahern and Derek R. Laver
John Curtin School of Medical Research, Australian National University, Canberra ACT 2601, Australia

ABSTRACT We describe ATP-dependent inhibition of the 75–105-pS (in 250 mM Cl^-) anion channel (SCl) from the sarcoplasmic reticulum (SR) of rabbit skeletal muscle. In addition to activation by Ca^{2+} and voltage, inhibition by ATP provides a further mechanism for regulating SCl channel activity in vivo. Inhibition by the nonhydrolyzable ATP analog 5′-adenylylimidodiphosphate (AMP-PNP) ruled out a phosphorylation mechanism. Cytoplasmic ATP (~1 mM) inhibited only when Cl^- flowed from cytoplasm to lumen, regardless of membrane voltage. Flux in the opposite direction was not inhibited by 9 mM ATP. Thus ATP causes true, current rectification in SCl channels. Inhibition by cytoplasmic ATP was also voltage dependent, having a K_i of 0.4–1 mM at −40 mV (Hill coefficient ~2), which increased at more negative potentials. Luminal ATP inhibited with a K_i of ~2 mM at +40 mV, and showed no block at negative voltages. Hidden Markov model analysis revealed that ATP inhibition 1) reduced mean open times without altering the maximum channel amplitude, 2) was mediated by a novel, single, voltage-independent closed state (~1 ms), and 3) was much less potent on lower conductance substates than the higher conductance states. Therefore, the SCl channel is unlikely to pass Cl^- from cytoplasm to SR lumen in vivo, and balance electrogenic Ca^{2+} uptake as previously suggested. Possible roles for the SCl channel in the transport of other anions are discussed.

INTRODUCTION

The sarcoplasmic reticulum (SR) of striated muscle is specialized for the uptake, storage, and release of Ca^{2+} ions, which initiate contraction. The key components of this system are the ryanodine receptor (RyR) responsible for calcium release (for a review see Coronado et al., 1994) and Ca^{2+} ATPase, which pumps Ca^{2+} back into the SR lumen. The SR also contains a large conductance K^+ channel, which has been extensively studied (Coronado et al., 1980; Miller and Racker, 1976), and several types of anion channels of unknown function. We have recently described properties of a large-conductance (~250 pS, 250 mM Cl^-) Cl^- channel (BCl) and a small-conductance (~75–105 pS) Cl^- channel (SCl) in SR vesicles from rabbit skeletal muscle (Kourie et al., 1996a,b). In lipid bilayers, the BCl channel is mostly open and is insensitive to both changes in voltage and cytoplasmic [Ca^{2+}], similar to a previously described SR anion channel (Hamilton et al., 1989; Kourie et al., 1996b; Sukhareva et al., 1994; Tanifuji et al., 1987). In contrast, the SCl channel appears to be a novel SR channel. It is sensitive to voltage and responds rapidly and reversibly to changes in cytoplasmic Ca^{2+}; the [Ca^{2+}] threshold for channel opening is ~1 μM, and channels reach maximum activation at ~100 μM. Thus the channel is potentially active in the range of [Ca^{2+}] in the myoplasm during muscle contraction (Ruegg, 1988).

Although the functions of SR Cl^- channels are unclear, one role may be to provide a counter-current to Ca^{2+} flux and clamp the potential difference (PD) across the SR close to its resting value of approximately zero (Fink and Veigel, 1996). In principle, both Ca^{2+} release and uptake will generate a large PD across the SR. Indeed, Ca^{2+} ATPase is known to be electrogenic, producing a PD of ~−60 mV in artificial vesicles (cytoplasm to lumen; Zimniak and Racker, 1978), which if left uncompensated in vivo would tend to oppose Ca^{2+} uptake. Thus neutralization of the electrogenic pump by counter-transport of H^+ (Yu et al., 1994) or K^+/Cl^- flux across the SR would maintain the PD at close to zero and facilitate Ca^{2+} uptake. Accordingly, inhibition of anion channels in pancreatic endoplasmic reticulum (ER) impairs Ca^{2+} uptake (Kemmer et al., 1987). Likewise, Ca^{2+} release will also generate a large PD across the SR but with a sign opposite that of Ca^{2+}-uptake. This PD is most likely neutralized by cation movement into the SR, either through the RyR itself (K^+, H^+, or Mg^{2+} ions) or through K^+ channels (see Fink and Veigel, 1996). Electron probe analysis has shown that K^+ and Mg^{2+} ions do move into the SR during tetanic stimulation, but that the movement of these cations does not fully balance Ca^{2+} release (Somlyo et al., 1981). Thus the charge deficit must be compensated by other ions. Interestingly, Somlyo et al. reported no redistribution of Cl^- ions, arguing against a role for Cl^- in charge compensation. Although both Ca^{2+}-induced Ca^{2+} release and voltage-activated Ca^{2+} release are enhanced (Ikemoto et al., 1994; Sukhareva et al., 1994) in the presence of supraphysiological Cl^- (150 mM; cf. ~7 mM in rabbit), it is not clear whether this is due to Cl^- acting as a counterion or to a direct activation of the RyR by Cl^- ions (Fruen et al., 1996; Meissner et al., 1997).

Received for publication 10 November 1997 and in final form 31 January 1998.

Address reprint requests to Dr. Gerard Ahern, Department of Physiology, SMI 129, University of Wisconsin-Madison, 1300 University Ave., Madison, WI 53706. Tel.: 608-262-9112; Fax: 608-265-5512; E-mail: gahern@facstaff.wisc.edu.

0006-3495/98/05/2335/17 $2.00

We have previously suggested that the SCl channel, because of its voltage characteristics and activation by Ca^{2+}, may provide a counterion current to balance Ca^{2+} uptake, similar to anion channels in the ER of the pancreas. However, the function of the SCl channel is unclear, because of the high Cl^- permeability through BCl channels, which would overwhelm current passed by SCl channels. It is possible that a physiological role of SCl channels involves the movement of other anions across the SR, including inorganic phosphate and ATP. Recently, the voltage-dependent anion channel (VDAC), normally thought to be in the mitochondrial outer membrane, has been detected by immunostaining in SR (Junankar et al., 1995; Shoshan-Barmatz et al., 1996). VDAC channels have been shown to be permeable to ATP (Rostovtseva and Colombini, 1997) and have been postulated by Shoshan-Barmatz et al. to allow passage of ATP into the SR lumen, allowing phosphorylation of intraluminal proteins. It is possible that SCl channels may also play a role in metabolite transport.

We now report that SCl channel activity in lipid bilayers is inhibited by submillimolar concentrations of adenine nucleotides, which confirms the findings of a recent study (Kourie, 1997). Furthermore, we show that ATP inhibition is dependent on the direction of the net Cl^- flux, such that *cis* ATP only inhibits fluxes from *cis* to *trans* compartments; thus ATP induces a true current rectification of the SCl channel. In addition, *cis* ATP inhibition is relieved at more negative PDs, which is inconsistent with a simple ion block mechanism, raising the possibility that ATP permeates the SCl channel. Finally, using hidden Markov model (HMM) signal analysis methods, we find that ATP has differential effects on channel conductance levels. Our results suggest that under normal physiological conditions, adenine nucleotides in the cytoplasm will inhibit Cl^- flux from cytoplasm to SR lumen, but not in the opposite direction, and therefore SCl channels are unlikely to contribute to the counterion pathway that balances Ca^{2+} uptake, as previously suggested.

MATERIALS AND METHODS

Isolation of terminal cisternae membranes

SR vesicles were prepared as previously described (Ahern et al., 1994; Laver et al., 1995), using methods based on the work of Saito et al. (1984). Back and leg muscles were dissected from New Zealand rabbits, snap frozen in liquid N_2, and stored at -70°C. Frozen cubes of muscle were pulverized and homogenized in buffer A (mM: 20 imidazole, 300 sucrose, adjusted to pH 7.4 with HCl). Terminal cisternae vesicles were collected from the 38–45% (w/w) interface of a discontinuous sucrose gradient after centrifugation. All procedures were performed at 4°C, and buffers contained the protease inhibitors leupeptin (1 μM), pepstatin A (1 μM), benzamidine (1 mM), and phenylmethylsulfonyl fluoride (0.7 mM).

Chemicals

Stock solutions (50–500 mM) of ATP, Mg^{2+}, or Na^+ salt, and 5′-adenylylimidodiphosphate (AMP-PNP), Li^+ salt (Sigma) were prepared in 250 mM CsCl and 10 mM *N*-tris-(hydroxymethyl)methyl-2-aminoethanesulphonic acid (TES), pH 6–7, and stored at -70°C. In bilayer experiments adenine nucleotide concentrations were adjusted by adding aliquots of stock solutions to the *cis* or *trans* chamber, or by perfusing the chambers with CsCl/ATP (pH 7.5) solutions buffered to 1 mM free Ca^{2+}, using a Ca^{2+}-selective electrode (ION83 Ionmeter; Radiometer, Copenhagen). The addition of stock ATP solution (pH 6) at up to 2 mM final concentration shifted pH by less than 0.01 units. Concentrations of free Ca^{2+} and ATP complexes were estimated by using published association constants (Marks and Maxfield, 1991) and the program *Bound and Determined* (Brooks and Storey, 1992).

Artificial lipid bilayers

Lipid bilayers of palmitoyl-oleoyl-phosphatidylethanolamine, palmitoyl-oleoyl-phosphatidylserine, and palmitoyl-oleoyl-phosphatidylcholine (5:3:2 w/w; Avanti Polar Lipids, Alabaster, AL) were formed over ~250-μm-diameter apertures in the wall of 1.5-ml delrin cups. Terminal cisternae vesicles were added to the *cis* chamber to a final concentration of ~10 μg/ml. Standard solutions were 250/50 mM CsCl *cis*/*trans*, with 1 mM $CaCl_2$ and 10 mM TES, pH 7.5, *cis/trans.* For current reversal and voltage experiments, solutions containing 250/250, 250/500, or 250/1000 mM CsCl *cis*/*trans* were used.

Recording single-channel activity

Voltage was controlled and current recorded at 20–25°C via an Axopatch 200 amplifier (Axon Instruments, Foster City, CA). Potentials are given with respect to the *trans* chamber. Unless otherwise stated, SCl channel activity was recorded at -40 mV after a brief (~1 s) prepulse to $+40$ mV, used to remove the voltage-dependent inactivation of channel activity that occurs at negative potentials (Kourie et al., 1996a). Channel activity was filtered at 1 or 2.5 kHz and digitized at 2 or 5 kHz. Preliminary analysis of single-channel records was made using an in-house computer program (*Channel2*; M. Smith and P. W. Gage). Parameters measured were T_o (the mean open time), P_o (the sum of open times divided by total time), and I'/I_{max} (the time-averaged current divided by the maximum current). These parameters were calculated from channel activity within bursts to avoid variability arising from long closures between bursts. The effects of adenine nucleotides on the burst properties of the channels were calculated using an interburst gap threshold of 50 ms. This threshold interval was chosen because it was much longer than that expected for ATP-induced closed events. Average parameter values are given as mean $\pm$ 1 SEM. Current amplitude levels were initially measured using mean-variance analysis (Patlak, 1988), as previously described (Ahern et al., 1997).

Identification of SCl channels

SCl channels were readily distinguished from other SR channels by the following properties: their selectivity for Cl^- over Cs^+ (average reversal potential ~$+30$ mV in 250/50 mM CsCl), conductance that varies between 70 and 105 pS (in 250/50 mM CsCl), activation by Ca^{2+} (>1 μM), and inactivation at sustained negative voltage as previously described (Kourie et al., 1996a,b).

Hidden Markov model algorithm

Detailed analysis of channel open, substate, and closed durations was made using the HMM algorithm (Chung et al., 1990, 1991). HMM finds the maximum likelihood estimate of the channel current transitions present in the record (i.e., an idealized representation of the recording) and provides for the determination of channel substate amplitudes and probabilities and transition rates. It is based on the assumption that the channel current signal is the sum of a first-order finite-state Markov process and white, uncorrelated Gaussian noise of known variance. Analysis was carried out on single-channel recordings, with steady baseline, varying in duration from

10 to 60 s and containing between 10^3 and 10^4 events. To satisfy the HMM assumptions, the current signal was slightly undersampled (replayed at 1 or 2.5 kHz and digitized at 2 or 5 kHz) to eliminate any correlation between adjacent data points. Unlike other channel analysis algorithms, the accuracy of HMM is not diminished by undersampling, because the effects of discrete data sampling are taken into account by the algorithm.

Analysis of dwell times

Dwell-time frequency histograms of channel open, closed, and substates were compiled from idealized representations of the data that were created by HMM. The distributions are displayed as the number of events of a particular duration per second of recording, and the data are plotted using the "log-bin" method suggested by Sigworth and Sine (1987). Putative models for ATP inhibition were evaluated by fitting theoretical probability distribution functions (PDFs) to the dwell-time histograms by using the Q-matrix method (Colquhoun and Hawkes, 1981). The algorithm of Blatz and Magleby (1986) was used to calculate the effects of current steps that were too short to be detected. For current records that were filtered at 2.5 kHz, the detection limit (dead time) of channel events was 200 μs.

Determination of transition rates between conductance states

The transition probability matrix, **P**, created by HMM summarizes the Markov statistics of the channel signal. The elements of this matrix, $\mathbf{P}_{ij}$, give the probability of a transition occurring between states i and j in a single sample interval. The matrix of rate constants for transitions between conductance states of the channel, **Q**, was calculated from the transition probability matrix, **P**, using the equation

$$\mathbf{Q} = -\log[\mathbf{P}]/\Delta t$$

where Δt is the data sample interval. It greatly simplified the interpretation of the analysis when the many substates were grouped into a smaller number of compound states (e.g., channel openings that consist of times when the channel is in any of the nonzero conducting states). Transition rates into and out of compound states were calculated from a reduced transition probability matrix derived from **P** by a method given by Chung and Kennedy (1996).

Modeling SCl channel dwell times

The kinetics of ATP inhibition are consistent with a binding reaction in which ATP-induced closed intervals are periods during which one or more ATP molecules either block the pore or are bound to regulatory sites on the channel protein (see Discussion). From this model the rates for the binding and unbinding of ATP are derived from the frequency and duration of the ATP-induced channel closures. We consider two models in which the binding of two or more adenine nucleotide molecules to the channel protein causes immediate closure of the pore.

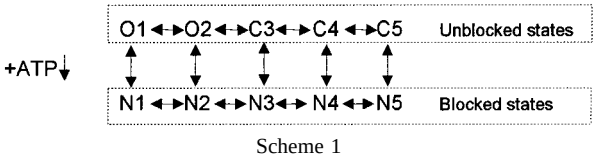

Scheme 1

In Scheme 1 ATP binding is independent of the state of the channel. The scheme for the unblocked states incorporates two open states and three closed states to accommodate the number of exponentials seen in the dwell-time distributions. The reaction rates between states N1 and N5 are the same as those between states O1 and C5, respectively. ATP binds to the channel independently of the open or closed state of the pore. Initially, Scheme 1 was fitted with the control to derive the reaction rate constants between the unblocked states. Scheme 1 was then fitted with ATP channel data by varying only the ATP binding and unbinding rate parameters. Another ATP binding model (Scheme 2) was also considered and fitted with dwell-time data. Scheme 2 was the same as Scheme 1, except that ATP can only bind to the open channel.

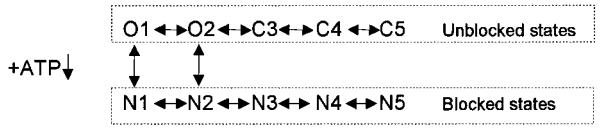

Scheme 2

Testing outcomes of analysis using simulations of raw data

Because single-channel recordings are unavoidably corrupted by background random noise and limited recording bandwidth, the analysis and modeling techniques can only provide an approximate measure of the channel gating properties. The HMM algorithm determines the most likely channel gating properties given the current recordings. However, because of noise and filtering, the most likely answer is not necessarily the true answer. Therefore, in this paper we tested the important conclusions of the signal analysis by using a simulation method. Model channel signals, incorporating the hypotheses to be tested, were embedded in white noise and filtered to simulate real single-channel records. Both the simulated and authentic records were analyzed in the same way, so that when the authentic and synthetic records matched, the analysis artifacts would be the same and the effects of artifacts would cancel out when the results from the authentic and synthetic records were compared. Thus the advantage of this approach is that it is relatively insensitive to analysis artifacts. Simulated recordings of ATP-inhibited channels were constructed from authentic control experimental records and the putative inhibition model, as shown in Fig. 1. The HMM algorithm was used to make an idealized representation of the authentic control records. The effect of ATP in the idealized signal was simulated by replacing sections of the waveform with channel closures at stochastic intervals. The timing of these intervals was determined by the ATP binding and unbinding rate constant parameters and a series of random numbers generated from a BASIC program. The ATP-inhibited idealized signal was filtered in the same way as the authentic records and combined with baseline noise, which was obtained from sections of the control recording.

RESULTS

Adenine nucleotide block

Addition of ATP (either the magnesium or sodium salt, 0.1–5 mM) to the cytoplasmic face of Ca^{2+}-activated SCl channels (1–10 mM Ca^{2+}) produced an immediate decrease in channel open probability measured within bursts (n = 23). An example of ATP inhibition is shown in Fig. 2 *A* (*left*). Under control ATP-free conditions with 1 mM activating Ca^{2+}, the P_o and mean open time (T_o) within a burst of openings were 0.94 and 23.0 ms (*upper trace*); however, these values fell to 0.42 and 1.2 ms after the addition of 1 mM Na_2ATP to the *cis* chamber (*middle trace*). P_o and T_o were returned toward control values (0.79, 5.7 ms) after the *cis* chamber was perfused with an ATP-free solution (*bottom trace*). Block of SCl channel activity was also seen after the addition of the nonhydrolyzable ATP analog AMP-PNP (n = 6, Fig. 2 *A*, *right*) in Mg^{2+}-free conditions. In this channel values for P_o and T_o were reduced from 0.82 and 11.0 ms to 0.42 and 1.1 ms, respectively, after the addition of 0.33 mM Li_2AMP-PNP. Washout of the *cis* chamber

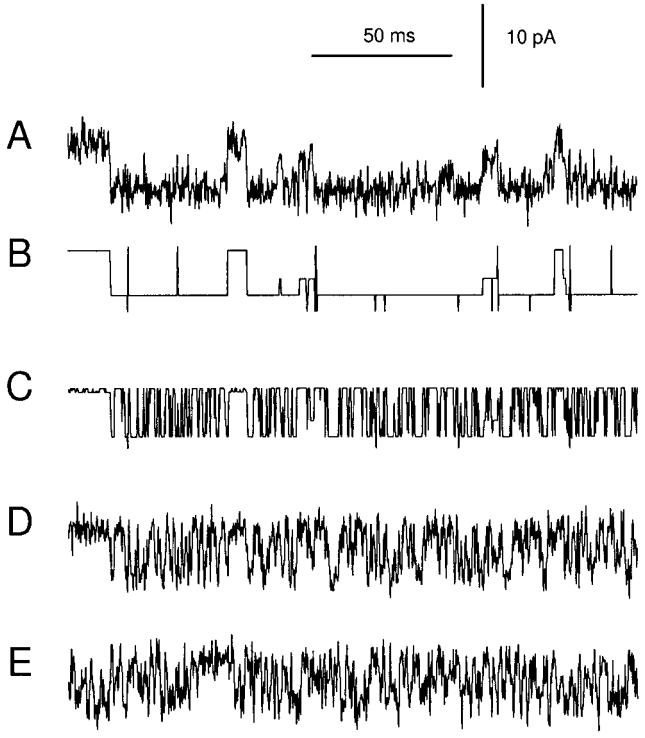

FIGURE 1 The steps involved in producing simulated recordings of ATP-inhibited SCl channels. (*A*) Recording of an uninhibited SCl channel at −40 mV. The baseline is toward the top of each trace, and channel openings are shown as downward current steps. (*B*) The raw data were analyzed by the HMM algorithm to produce an idealized representation of the control signal with current levels at 0, −0.5, −4, −6, and −8 pA. (*C*) Simulated ATP inhibition of the idealized signal was achieved by replacing sections of the waveform in *B* with channel closures at stochastic intervals. The ATP-inhibited idealized signal was filtered at 2.5 kHz. (*D*) The signal in *C* was superimposed on another signal consisting of baseline noise, which was obtained from sections of the control recording in *A*. The resulting signal (the simulated record) was analyzed in the same way as the authentic recording of the ATP-inhibited channel, which is shown in record *E*.

with AMP-PNP-free solution increased P_o and T_o to 0.78 and 5.4 ms, respectively. Although Li_2AMP-PNP appears in Fig. 2 *A* to be a more potent inhibitor of channel activity than Na_2ATP, this was a consequence of channel-to-channel variability (see below). There was little difference in the potency of these compounds seen in averaged data (see Fig. 2 *C*). The block by AMP-PNP indicates that inhibition by ATP is independent of channel phosphorylation and occurs at an adenine-nucleotide binding site. In addition, we found that channel activity was unaffected by perfusion of the *cis* chamber with a solution containing 10 mM HPO_4^{2-} (inorganic phosphate), indicating that the charge of a single phosphate group was not sufficient to induce inhibition.

To examine the effects of adenine nucleotides on relatively slow channel gating, we measured burst durations (bursts were defined as groups of openings separated by closures of >50 ms; see Materials and Methods) and intervals between bursts for up to 60 s after a voltage step from +40 to −40 mV. Adenine nucleotides (0.33–1.6 mM) reduced burst durations in 12/12 channels by 75 ± 5% and reduced intervals between bursts in 9/12 channels by 48 ± 8%.

Dose dependence of adenine nucleotide block

Fig. 2 *B* shows the effect of varying *cis* [ATP] at −40 mV on the activity of a single SCl channel. MgATP inhibited activity in a dose-dependent manner; under control conditions with 2.3 mM activating Ca^{2+}, P_o was 0.87, but fell to 0.58, 0.20, and 0.04, respectively, after [MgATP] was increased successively to 0.66, 1.66, and 2.66 mM. Fig. 2 *C* summarizes the relationship between normalized P_o ($P_{oATP}/P_{oControl}$) and [adenine nucleotide] in experiments that used MgATP ($n = 4$), Na_2ATP ($n = 9$), or Li_2AMP-PNP ($n = 5$). Open probability was measured by using a threshold detection set at half the maximum open amplitude, and for simplicity of analysis we did not include channel activity that contained pronounced subconductance activity (substate modes). The effects of ATP on these substate modes is studied separately in a later section. The lines are least-squares fits to Eq. 1 (see legend to Fig. 2 *C*). The concentrations for half-maximum block (K_I) and the Hill coefficients (H) were 0.45 ± 0.06 mM and 1.7 ± 0.4 for Na_2ATP, 0.95 ± 0.05 mM and 2.6 ± 0.4 for MgATP, and 0.32 ± 0.03 mM and 1.5 ± 0.3 for Li_2AMP-PNP. There was significant channel-to-channel variation in sensitivity to ATP inhibition, for individual channels K_I for *cis* Na_2ATP ranging from 0.29 mM to 0.90 mM (mean = 0.53, SD = 0.22; $n = 7$). Activity was also measured by the mean-current method, which gave results similar to those of P_o analysis ($K_I = 0.32$ mM, and H ranging from 1.5 to 2.7 for five channels inhibited by Na_2ATP). Our results also show that ATP and AMP-PNP block from the *trans* side of the bilayer, but with less potency than the *cis* side (see below).

The interpretation of the dose-response relationships is complicated by the fact that the proportions of the various ATP complexes and the free [Ca^{2+}] and [ATP] could not be held constant in these experiments. Hence values for K_I and Hill coefficient may represent an averaged response of the channel to these differently charged ionic species. In this case K_I values would still be physiologically relevant, because these ATP complexes exist in vivo, but the interpretation of the Hill coefficients would be limited. The problem of ATP complexation is addressed in detail in the Discussion.

Voltage dependence of *cis* ATP inhibition

Fig. 3 shows the effect of 1 mM *cis* ATP on SCl channel activity recorded at different bilayer potentials, ranging from +60 mV to −80 mV (data at 0 mV to −80 mV are from the same channel in 250/50 mM *cis*/*trans* CsCl and inhibited with MgATP; data at positive potentials are from different channels in symmetric 250/250 mM *cis*/*trans* CsCl solution and inhibited by Na_2ATP). ATP had little effect on P_o at +60 and +40 mV. In contrast, at potentials less than or equal to 0 mV, ATP produced a marked inhibition of

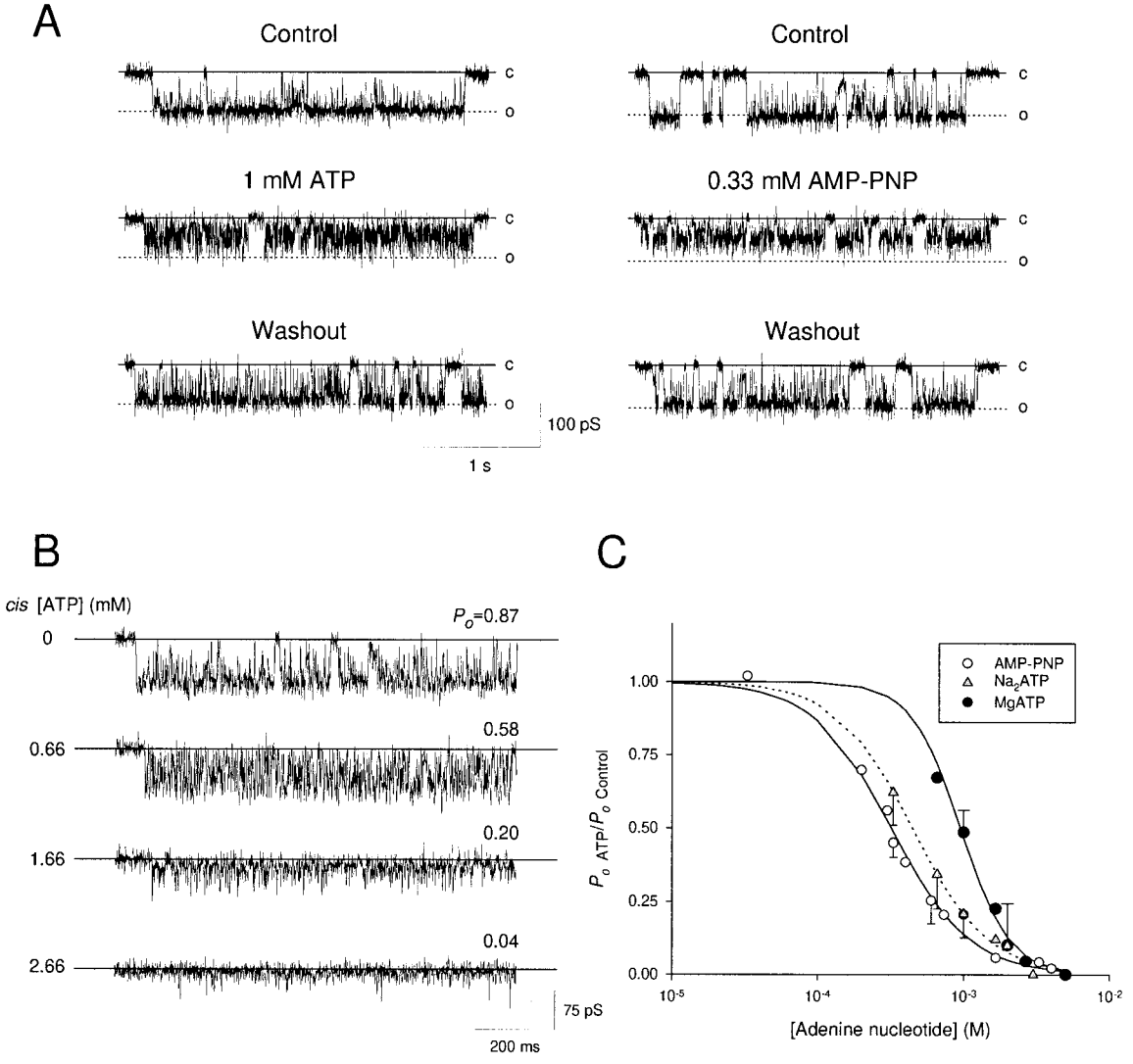

FIGURE 2 Adenine nucleotides inhibit SCl channel activity. (*A*) Representative channel activity recorded with a bilayer potential of −40 mV (relative to *trans*). The solid and dotted lines indicate the closed and open levels, respectively, measured under control conditions. *Left*: Channel activity before (*top*) and after the addition of 1 mM Na_2ATP (*middle*) and after perfusion with an ATP-free solution (*bottom*). *Right*: Activity from a separate channel before (*top*) and after the addition of 0.33 mM of the nonhydrolyzable ATP analog AMP-PNP (Mg^{2+} free conditions) to the *cis* chamber (*middle*) and after perfusion with an AMP-PNP-free solution (*bottom*). Note that in both experiments total [Ca^{2+}] was 1 mM, and free Ca^{2+} estimated with the BAD computer program (see Materials and Methods) was much greater than the 100 μM required for maximum channel activation. (*B*) Representative current traces from a single SCl channel with 0.66–2.66 mM MgATP, as indicated on the left. The bilayer potential was −40 mV, and total *cis* Ca^{2+} was 2.3 mM (free Ca^{2+} was >1 mM in each case). P_o calculated from several bursts of channel activity is given at the top right of each trace. (*C*) Plot of normalized P_o ($P_{oATP}/P_{oControl}$) versus either [Li_2AMP-PNP] (○, n = 5), [Na_2ATP] (△, n = 9), or [MgATP] (●, n = 4). Data were filtered at 1 kHz and digitized at 2 kHz. P_o was measured at −40 mV, and the detection threshold for events was set at half the maximum amplitude for each condition. Data points with error bars are mean values ± 1 SEM, and lines are best fits to Eq. 1:

$$\frac{P_{o(ATP)}}{P_{o(Control)}} = \frac{1}{1 + \left(\frac{[\text{adenine nucleotide}]}{K_I}\right)^H} \quad (2)$$

where K_I is the concentration of adenine nucleotide producing half-maximum inhibition, and H is the Hill coefficient. Values for K_I and H are given in the text.

activity, but the inhibition was attenuated with increasing negative voltage; at 0 mV P_o decreased from 0.60 to 0.04, whereas at −80 mV P_o decreased from 0.55 to 0.44. Note that Cl^- current flows from *trans* to *cis* at positive potentials and from *cis* to *trans* at negative potentials. Fig. 4 *A* summarizes the relationship between P_o and bilayer potential before and after inhibition by 1 mM ATP. Before ATP application, P_o measured within bursts was generally high at all potentials (note that the voltage dependence described in our previous studies arises from the voltage dependence of

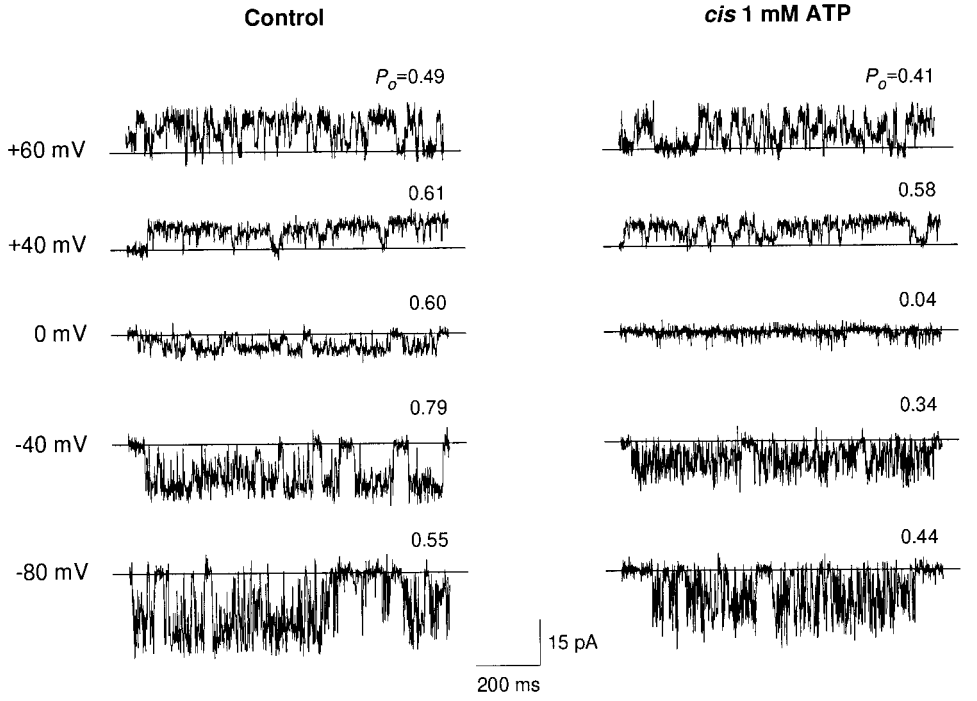

FIGURE 3 Voltage dependence of inhibition by *cis* ATP. Representative current traces at different bilayer potentials before (*left*) and after (*right*) the addition of 1 mM ATP. P_o calculated from within bursts of channel activity lasting several seconds is given above each trace. Activity at 0 to −80 mV was recorded from a single channel with 250/50 mM CsCl in the presence of 1 mM MgATP; activity at +40 mV and +60 mV was recorded from different channels with symmetrical 250 mM *cis*/*trans* CsCl in the presence of 1 mM Na_2ATP.

burst frequency). ATP produced little or no inhibition at +40 mV, but substantial inhibition at 0 mV, which became less pronounced with increasing negative potential. The effect is well illustrated by a plot of normalized P_o ($P_{o\ ATP}/P_{o\ Control}$) versus voltage (Fig. 4 *B*). The circles and triangles show data for *cis* ATP inhibition in 250/50 and 250/250 CsCl, respectively. The inhibition produced by 1 mM MgATP decreases at more negative PDs over the range 0 mV to −80 mV. K_I at −80 mV (~2 mM) was about twofold higher than at −40 mV (~0.95 mM), which was, in turn, about two- to threefold higher than at 0 mV (~0.3–0.4 mM), and there was no significant inhibition at positive potentials. The voltage dependence over the range 0 mV to −80 mV is opposite that expected for a simple voltage-dependent blocking mechanism, in which a negative potential difference drives ATP onto the channel pore and inhibits the channel, and positive potentials relieve the block. In contrast, the results here (0 mV to −80 mV) show that ATP inhibition is relieved by increased negative voltage. Our results described below suggest that the relief of ATP inhibition at positive potentials seen in Fig. 4 *B* is not due to voltage per se, but to the direction of the Cl^- flux.

ATP inhibition is dependent on the direction of the Cl^- flux

The sharp discontinuity in the P_o-voltage plot shown in Fig. 4 *B* between negative and positive potentials occurs close to the reversal potential under these conditions and indicates that ATP inhibition may be influenced by the direction of Cl^- current. To investigate this possibility, we altered the *trans* solution composition to measure the effect of current direction on ATP inhibition, independently of voltage. Fig. 5 *A* shows that 1 mM *cis* ATP nearly completely inhibited SCl channel activity at 0 mV when net current flowed from *cis* to *trans* (250/50 mM *cis*/*trans* CsCl), but up to 9 mM *cis* ATP did not inhibit activity at 0 mV when the current flowed in the opposite direction, from *trans* to *cis* (250/1000 mM *cis*/*trans* CsCl; see Fig. 5 *B*). We found that reversing the Cl^- current at 0 mV removed ATP inhibition in 3/3 channels (Fig. 5 *C*). Furthermore, we found that changing the Cl^- reversal potential caused a similar shift in the discontinuity in the P_o-voltage plot without significantly changing the potencies of ATP inhibition at either more positive or more negative potentials. Fig. 6 shows the P_o-voltage relationship for SCl channels inhibited by 1 mM *cis* ATP in either 250/50, 250/500, or 250/1000 mM *cis*/*trans* CsCl. It is clear that the channels were only inhibited at potentials more negative than the reversal potential (i.e., when current flowed from the *cis* to *trans* chamber). Thus *cis* ATP induces a *trans* to *cis* (inward) rectification of Cl^- flux. This result shows that the discontinuity in the P_o-voltage data (Fig. 6 *B*) is due to the Cl^- flux and not the membrane potential per se.

Voltage dependence of *trans* ATP inhibition

To further examine the *cis*/*trans* specificity of ATP action, we studied the effects of *trans* ATP on SCl activity. In 3/3 experiments, channel activity was inhibited by millimolar *trans* ATP or AMP-PNP in a voltage-dependent manner. Fig. 7 shows that whereas 1 mM *trans* Na_2ATP (in 50 mM *trans* Cl^-) substantially reduced channel P_o at +60 mV (from 0.81 to 0.49), it had little effect at negative potentials. The simple voltage dependence of *trans* ATP inhibition is similar to but opposite that of *cis* ATP, and is consistent

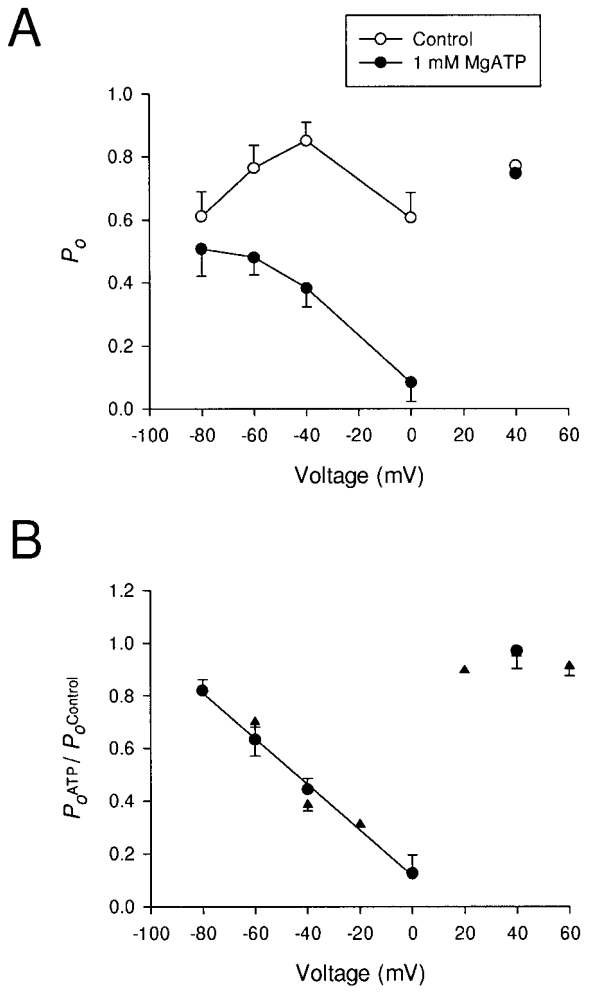

FIGURE 4 Plots of open probability versus voltage before and after 1 mM *cis* ATP. (*A*) Average P_o (± 1 SEM) versus bilayer potential, −80 mV ($n = 3$), −60 mV ($n = 5$), −40 mV ($n = 4$), 0 mV ($n = 4$), +40 mV ($n = 1$) before (○) and after (●) application of 1 mM MgATP. Solutions were 250/50 mM *cis*/*trans* CsCl. Note that there is little voltage dependence of activity under control conditions, because P_o was calculated within bursts and not from continuous channel activity (see Materials and Methods). (*B*) $P_{o\ ATP}/P_{o\ Control}$ versus voltage obtained from data in *A* (●). The solid line shows a near-linear decrease in inhibition over the range 0 to −80 mV. Data at positive potentials are also shown for channels inhibited by 1 mM *cis* ATP in symmetrical 250 mM CsCl (▲): −60 mV ($n = 2$), −40 mV ($n = 3$), −20 mV ($n = 1$), +20 mV ($n = 1$), +40 mV ($n = 4$), +60 mV ($n = 2$).

with *trans* ATP producing *cis* to *trans* (outward) rectification of Cl^- current. However, the potency of inhibition by *trans* Na_2ATP was considerably less than that by *cis* Na_2ATP. *Trans* Na_2ATP inhibited with $K_I \approx 2$ mM, at +40 mV ($n = 2$), compared to a $K_I \approx 0.45$ mM, at −40 mV, with *cis* Na_2ATP ($n = 9$).

Effects of adenine nucleotides on SCl channel conductance

Visual inspection and HMM analysis of SCl channel activity revealed between five and seven conductance levels similar to those seen in previous studies (Kourie et al., 1996a,b). The maximum likelihood amplitude histograms for SCl recordings produced by HMM showed a characteristic profile; a typical example is shown in Fig. 8. What normally appeared as a single broad peak in all-points and mean variance amplitude histograms (eg. Fig. 9) was revealed by HMM (Fig. 8) to be a band of at least three higher conductance substates between 50 and 100 pS. The SCl substates rapidly interchanged between these levels. Up to three lower conductance substates were also detected. A 20-pS substate was nearly always seen in SCl recordings and produced the prominent peak in the amplitude histograms near the baseline peak. The SCl channel would intermittently enter substate modes in which the current would step between the closed state and an open state in the range 15–40 pS (e.g., Fig. 9 *A*). These gating modes usually lasted from a few hundred milliseconds to several seconds.

The current traces in Fig. 2 *A* and the amplitude histograms in Figs. 8 and 9 show the effects of ATP on channel activity at various current levels. Although in Fig. 2 *A* it appears that both ATP and AMP-PNP reduced the apparent maximum current level of SCl channels, we found that this effect was probably due to a reduced mean channel open time and the frequency at which the data were filtered. Filtering at 1 kHz allowed for poor resolution of the shortened open events caused by adenine nucleotides. HMM analysis of data filtered at 2.5 kHz found that the amplitudes of the maximum current levels were relatively unaffected by ATP. Inhibition of channel P_o by up to 80% was associated with a reduction of less than 15% in the maximum current level. ATP increased the probability of the channel closed state by increasing the frequency of short (~1 ms) closures. HMM consistently identified an ATP-induced state with a conductance indistinguishable from zero (0.5 ± 0.5 pA; SD, $n = 5$) (see Fig. 8). The HMM algorithm was able to distinguish this new state because the algorithm can distinguish different channel states on the basis of their mean durations as well as their amplitude.

Even though HMM consistently identified the ATP-induced closed states and maximum current level, the amplitudes of the intermediate current levels could not be unambiguously identified in the presence of ATP. This was because the signal filtering that was necessary for maintaining a reasonable signal-to-noise ratio also blurred the rapid, ATP-induced current steps. However, it was obvious that within the intermittent, long substate modes, the SCl channel was less sensitive to blockade by adenine nucleotides than the higher conductance states. Fig. 9 shows examples of the differential sensitivity of current levels that can be seen in the SCl channel. In the channel shown in Fig. 9 *A* (*top trace*), activity before ATP addition was distributed among three conductance levels: a closed level at 0 pS, a prominent substate at 20 pS, and a high conductance level (O) centered about 71 pS. The proportion of activity at each level is displayed by the amplitude histogram (*right*) created by mean variance analysis of the data in the current trace. The lines in the current trace correspond to the peaks in the

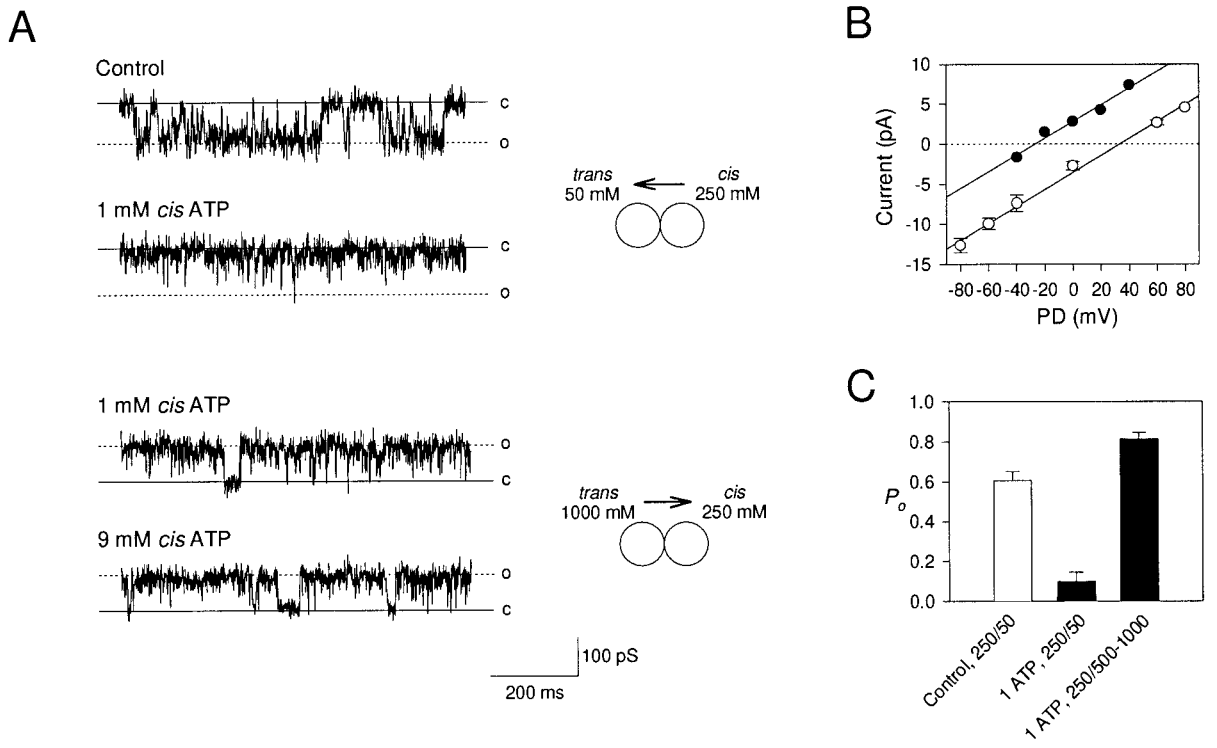

FIGURE 5 ATP inhibition is dependent on the direction of Cl^- flux. (*A*) Representative SCl channel activity inhibited by 1–9 mM *cis* MgATP. *Top*: Activity at 0 mV recorded with 250/50 mM *cis*/*trans* CsCl before and after addition of 1 mM *cis* MgATP; net Cl^- flux was from *cis* to *trans*. *Bottom*: Activity at 0 mV recorded with 250/1000 mM *cis*/*trans* CsCl and with either 1 or 9 mM *cis* MgATP; net Cl^- flux was from *trans* to *cis*. The solid line and dotted lines indicate the closed and open levels, respectively. (*B*) Current-voltage relationship for channels (absence of ATP) in 250/50 mM (○, n = 6) and 250/1000 mM (●) *cis*/*trans* CsCl. Increasing *trans* CsCl to 1 M shifted the reversal potential from +30 mV to −29 mV and reversed the direction of net current at 0 mV. (*C*) Open probability (mean ± 1 SEM) of SCl channels at 0 mV with either 250/50 mM CsCl, ATP-free (n = 4); 250/50 mM CsCl, 1 mM ATP (n = 6); or 250/500, 250/1000 mM CsCl, 1 mM ATP (n = 3). Note that inhibition by *cis* ATP was removed by reversing the direction of the Cl^- flux.

histogram. After the *cis* chamber was perfused with a solution containing 2 mM Na_2ATP buffered to 1 mM, free Ca^{2+} (*bottom*) activity to the maximum 71-pS level was nearly completely inhibited (note that sporadic openings to this level were too short to be detected by the mean variance analysis). In contrast, openings to the 20-pS substate level were unaffected by ATP. Fig. 9 *B* (*upper trace*) shows activity from a separate channel with a maximum conductance of 105 pS and a clear substate at ~42 pS. After the addition of 1 mM MgATP (*lower trace*), openings to the maximum 105-pS level and other levels were mostly blocked, whereas the 42-pS substate level was clearly less affected.

Effects of *cis* ATP on substate probabilities

A problem with measuring the effect of ATP inhibition on SCl substate probabilities and dwell times was that many of the substate current levels could not be determined with sufficient accuracy in the presence of ATP. Hence it was not possible to model the raw data in terms of a multilevel signal with accurately determined levels. The alternative of using a two-level (i.e., closed and open) signal to model the raw data was clearly inappropriate for the SCl channel, which has pronounced substate activity. Rather, the approach used here was to model the raw data in terms of a multilevel signal in which the current levels are set arbitrarily. Two idealized signal models were used to measure different aspects of ATP inhibition of SCl channels from the raw data.

Model 1 was designed to analyze the relatively fast, large current transitions between higher conductance substates and the closed states at membrane potentials between −80 and −40 mV. The model signal comprised a series of current levels at −4 pA, increasing in magnitude at 2-pA intervals (2.5-kHz filtering). Two types of channel closures were included in the model, namely, closures occurring in the absence of ATP (0 pA) and ATP-induced channel closures (−0.5 pA). The reason for the small nonzero value assigned to the ATP-induced closures was the need to distinguish them from the baseline in the idealized signal representations created by HMM. The number of levels used to model each record depended on the signal amplitude and varied from four to six. In this model the lower conductance substates are effectively lumped in with the channel ATP-independent closed state.

Model 2 was designed to analyze the relatively small, slow transitions between the lowest substate and the current

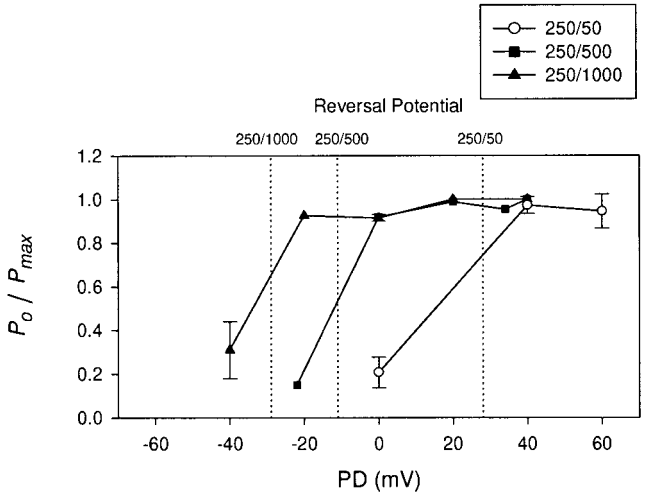

FIGURE 6 Discontinuity in the voltage dependence of ATP inhibition correlates with reversal potential. Plots of P_o/P_omax in 1 mM ATP (Na^+ or Mg^{2+} salt) versus voltage for channels in 250/50, 250/500, or 250/1000 mM *cis*/*trans* CsCl. Data are mean ± 1 SEM, and the dotted lines show reversal potentials for each condition (+30 mV, −11 mV, and −29 mV) estimated from plots of current versus voltage.

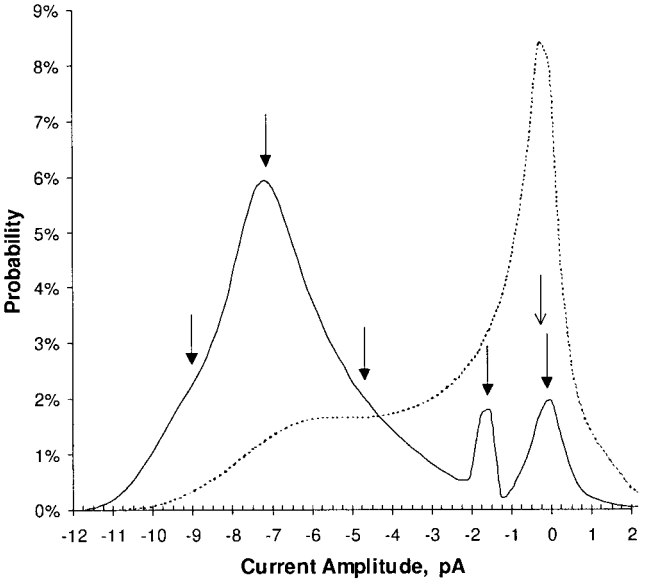

FIGURE 8 Maximum-likelihood histograms of amplitude probability of an SCl channel derived from the HMM algorithm. The histograms show the amplitude distributions in the absence of ATP (——) and in the presence of 2 mM *cis* MgATP (·····), which produced 80% inhibition of the channel. ATP does not reduce the maximum current. The single-channel recording was filtered at 2.5 kHz and was obtained at a membrane PD of −40 mV. The arrows point to current levels in the records identified by HMM. The light arrow points to a level that was consistently found only when ATP was present in the *cis* bath.

baseline (1-kHz filtering). SCl recordings were analyzed in terms of a three-level signal at −40 mV (0 pA, −2 pA, and another level between −5 and −7 pA, depending on the mean amplitude of the high conductance levels). The lower conductance level represents the substate, which was clearly identified in most SCl recordings because of its relatively long dwell time. The higher conductance level in the model is meant to account for the higher conductance substates of the SCl channel, which had very short dwell times in the presence of ATP. All recordings within each experiment were analyzed in terms of the same current levels.

Seven SCl recordings obtained at −40 mV and in the presence of various [ATP] were analyzed in terms of model 1 by using an idealized signal with current levels at 0, −4, −6, and −8 pA (50, 62, 100 pS). The effect of ATP on the substate probabilities and dwell times in a representative experiment is shown in Table 1. ATP appeared to have a more potent effect on the substate probabilities at −6 and −8 pA than at −4 pA. However, we show later (see Simulated ATP Inhibition) that ATP has the same inhibiting potency at these SCl substates and that the apparently differential effects of ATP on substates are probably an artifact of the limited bandwidth (2.5 kHz) of the channel recordings.

As mentioned above, the SCl channel normally showed substate distributions like that shown in Fig. 8 (normal gating mode), but occasionally also showed periods of pronounced substate activity (substate modes) lasting for hundreds of milliseconds to seconds. The substate modes of the SCl channel made it possible to separately measure the effects of ATP on probabilities and mean durations of the low- and high-conductance substates. Adenine nucleotide concentrations that produced ~90% inhibition of higher conductance states in normal mode gating had no effect on the open probability of the channel in its substate gating mode (n = 3; see Fig. 9). Because substates present in the SCl substate gating mode are insensitive to ATP, we examined the relative effects of ATP on the high- and low-

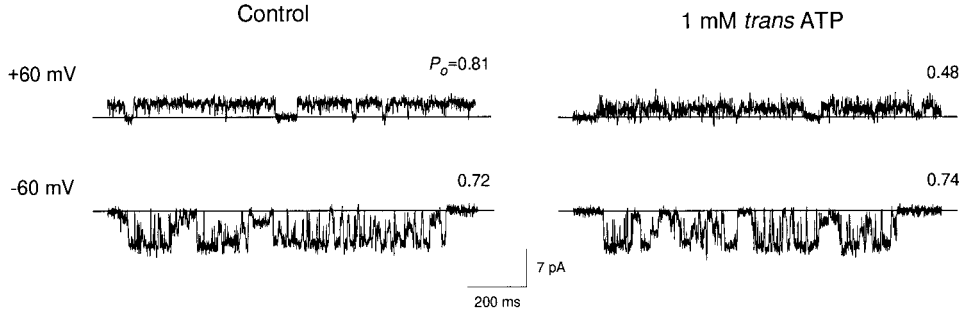

FIGURE 7 Voltage dependence of *trans* ATP block. Representative current traces from a single SCl channel before and after addition of 1 mM Na_2ATP to the *trans* chamber. The bilayer contained 250/50 mM *cis*/*trans* CsCl. *Trans* ATP inhibited the SCl channel at +60 mV but not at −60 mV. P_o values calculated from three or four bursts of channel activity are indicated above each trace.

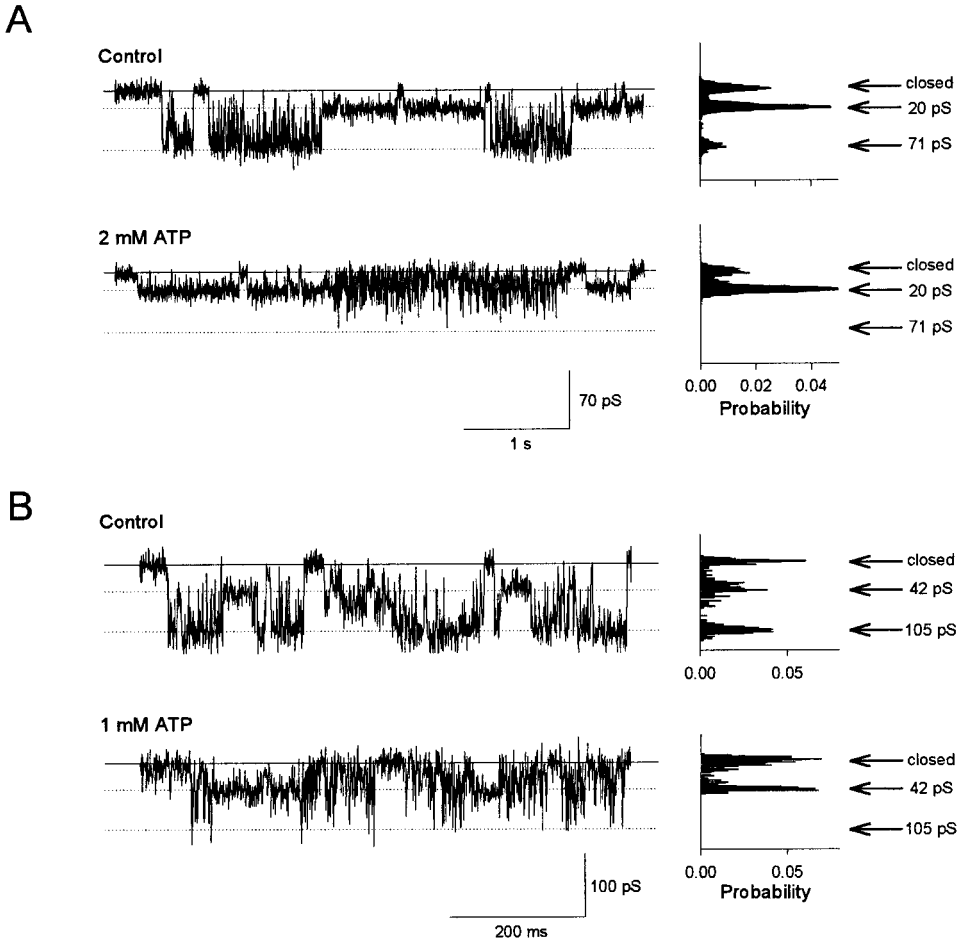

FIGURE 9 Differential ATP sensitivity of substates and the maximum open state. Data are from two SCl channel recordings selected to show the effect of ATP on prominent subconductance activity. Amplitude histograms constructed from mean variance analysis of the data in the traces are shown on the right. The lines in the current traces correspond to peaks in the amplitude histograms. Note that the maximum open levels are not resolved in the amplitude histograms after ATP treatment, and the arrows indicate the best estimate of their amplitude. (*A*) Before ATP application, current levels were observed at a closed level (0 pS), a substate (20 pS), and a maximum open level (71 pS). After the *cis* chamber was perfused with a solution containing 2 mM Na_2ATP and 1 mM free Ca^{2+}, activity to the maximum open level was mostly inhibited, whereas openings to the 20-pS level were unaffected. (*B*) A separate channel with a maximum conductance of 105 pS and a substate at 42 pS. Addition of 1 mM MgATP to the *cis* bath inhibited the maximum level, whereas the 42-pS substate was less affected.

conductance substates in the SCl normal gating mode ($n = 3$). This was measured by analyzing SCl recordings in terms of model 2, using an idealized signal with current levels at 0, −2 pA and another level between −5 and −7 pA. Table 2 shows the effect of ATP on the substate probabilities from one experiment. Whereas ATP decreased the probability of the high conductance level, it did not inhibit the 20-pS substate. We also show later (see Simulated ATP Inhibition) that this effect is consistent with ATP being a much less potent inhibitor of the 20-pS substate than in conductance states greater than 50 pS.

TABLE 1 The mean duration and probability of channel substates from the authentic and simulated recordings used in Fig. 9

[ATP], mM→	0	0.66	0.66	1.66	1.66
Substate level, pA	Data	Data	SIM	Data	SIM
Substate duration (ms)					
−4	0.56	0.32	0.29	0.12	0.13
−6	2.39	0.62	0.63	0.068	0.077
−8	0.081	0.058	0.041	0.048	0.036
Substate probability					
−4	0.13	0.13	0.12	0.1	0.1
−6	0.62	0.28	0.27	0.054	0.068
−8	0.083	0.049	0.05	0.008	0.012

ATP has a much stronger effect on the probabilities and durations of levels at −6 and −8 pA than at −4 pA. The simulated data (SIM) were constructed with the assumption that ATP has the same binding rate constant at all current levels of the channels.

Effects of *cis* ATP and voltage on substate durations

The effect of ATP on the dwell times in a representative experiment is shown in Table 1. ATP produced a larger

TABLE 2 The mean duration and probability of channel substates from authentic and simulated recordings

[ATP], mM→	0	2	2	2
Substate level, pA	Data	SIM1	Data	SIM2
Substate duration (ms)				
−2	0.83	0.37	0.64	0.83
−5	3.3	0.36	0.35	0.36
Substate probability				
−2	0.18	0.2	0.3	0.33
−5	0.56	0.09	0.07	0.09

The authentic data are compared with values obtained from records in which ATP inhibition is simulated in two ways. In SIM1, ATP binds with equal affinity with the channel in all conductance states. In SIM2, ATP only binds with the channel in the −5-pA state. The latter simulation produces a close match with the authentic data.

reduction in dwell times in the substate at −6 pA than at −8 pA and −4 pA. The mean open times of the SCl channel in its substate gating mode were unaffected by the presence of *cis* ATP up to 3 mM ($n = 3$). The relative effects of ATP on the high- and low-conductance substate dwell times were examined in three channels in their normal gating mode. The dwell times of the SCl channel at each conductance level were analyzed in terms of model 2. Table 2 shows the effect of ATP on the substate dwell times from one experiment. Two millimolar ATP caused a 10-fold reduction in the mean duration of the higher conductance levels, but had only a minor effect on the substate at 20 pS.

The effects of ATP on SCl gating between the high conductance substates and the closed state are studied here in detail. Substate transition rates and dwell times were estimated from the raw data by using model 2.

Conductance transition rates

The transition rates were derived from the maximum likelihood transition probability matrix describing the raw data determined by HMM (see Materials and Methods). ATP (~1 mM) increased, by 10–100-fold, the rate of current transitions from the higher substate levels to the −0.5-pA level, while producing only a small increase in the transition rate between the higher substates and the 0-pA level. ATP did not affect the reverse transition rates from either closed state to the higher conductance levels. Thus ATP had no significant effect on the native closed states of the channel, and the duration of ATP-induced closures was itself not dependent on [ATP].

Dwell-time distributions

The effects of ATP on SCl gating were studied again in greater detail by examining the dwell-time histograms of SCl substates. In compiling these histograms, closed intervals are defined as times when the current was at either the 0 or −0.5 pA level. Open intervals are defined as channel events consisting of any opening to the higher conductance substates (> −4 pA). Examples of such histograms are shown in Fig. 10 for channels in the absence of ATP. The closed dwell-time distributions clearly showed three exponential components, and the open dwell-time distributions showed two exponential components with time constants spanning the range 1–100 ms. Attempts to fit larger numbers of exponentials to the data provided only a marginal improvement in the quality of the fit parameter (the root mean square of the residuals). Fig. 11 shows the dwell-time distributions and analysis from an experiment that is representative of seven experiments that were analyzed in detail. The main effects of ATP were to shorten the open dwell times (Fig. 11, *B* and *D*) and to produce a marked increase in the frequency of ~1-ms closed events (Fig. 11 *C*). The frequencies of closed durations longer than 10 ms were unaffected. These ATP-induced closures could be accurately fitted with a single exponential ($\tau = 1.1$ ms; not shown). The time constant of the ATP-induced exponential component was relatively insensitive to the ATP concentration, only showing an increase at channel inhibition greater than >80%. The addition of ATP produced a marked decrease in the mean open time and altered the open time distribution so that only one exponential component was apparent.

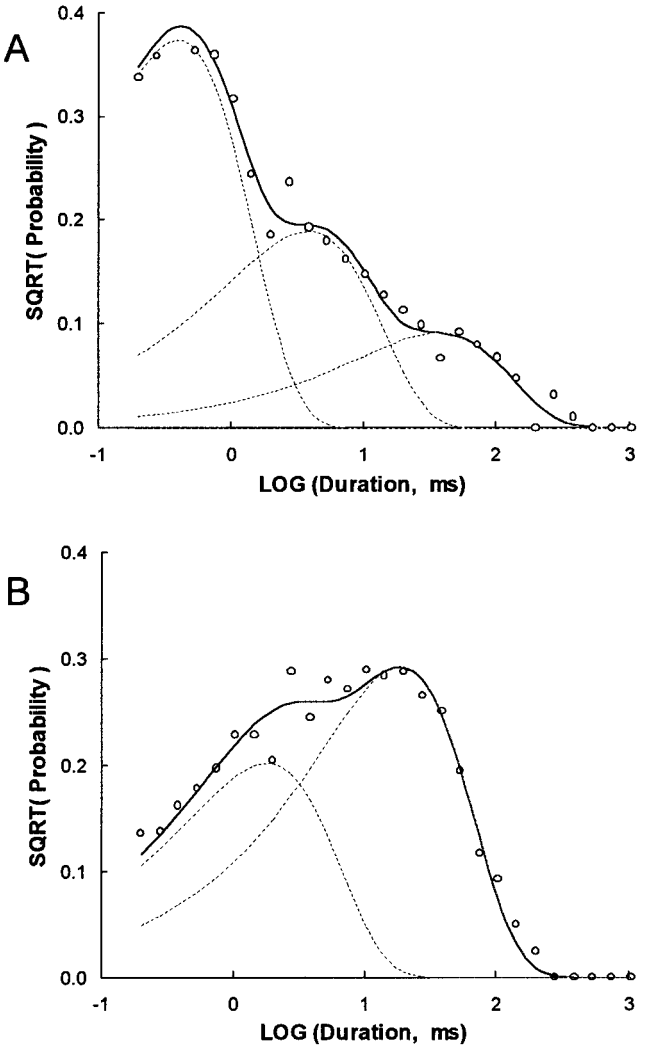

FIGURE 10 Dwell-time histograms of closed (*A*) and open (*B*) events for an SCl recorded at −40 mV. The data are displayed using the log-bin method employed by Sigworth and Sine (1987). The solid curves show multiexponential, least-squares fits to the data. The dashed lines show the different exponential components of the fit.

A simple binding mechanism could account for the dwell-time histograms of ATP-inhibited SCl channels. Channel open and closed dwell-time distributions were fitted with theoretical probability distribution functions, calculated from Scheme 1 (Fig. 11, *A* and *B*) and Scheme 2 (not shown) as described in Materials and Methods. Schemes 1 and 2 gave very similar predictions, which fitted well with most features on the dwell-time distributions (Fig. 11. *A* and *B*). Hence it was difficult to distinguish, from the frequency distributions, whether ATP binds to the channel

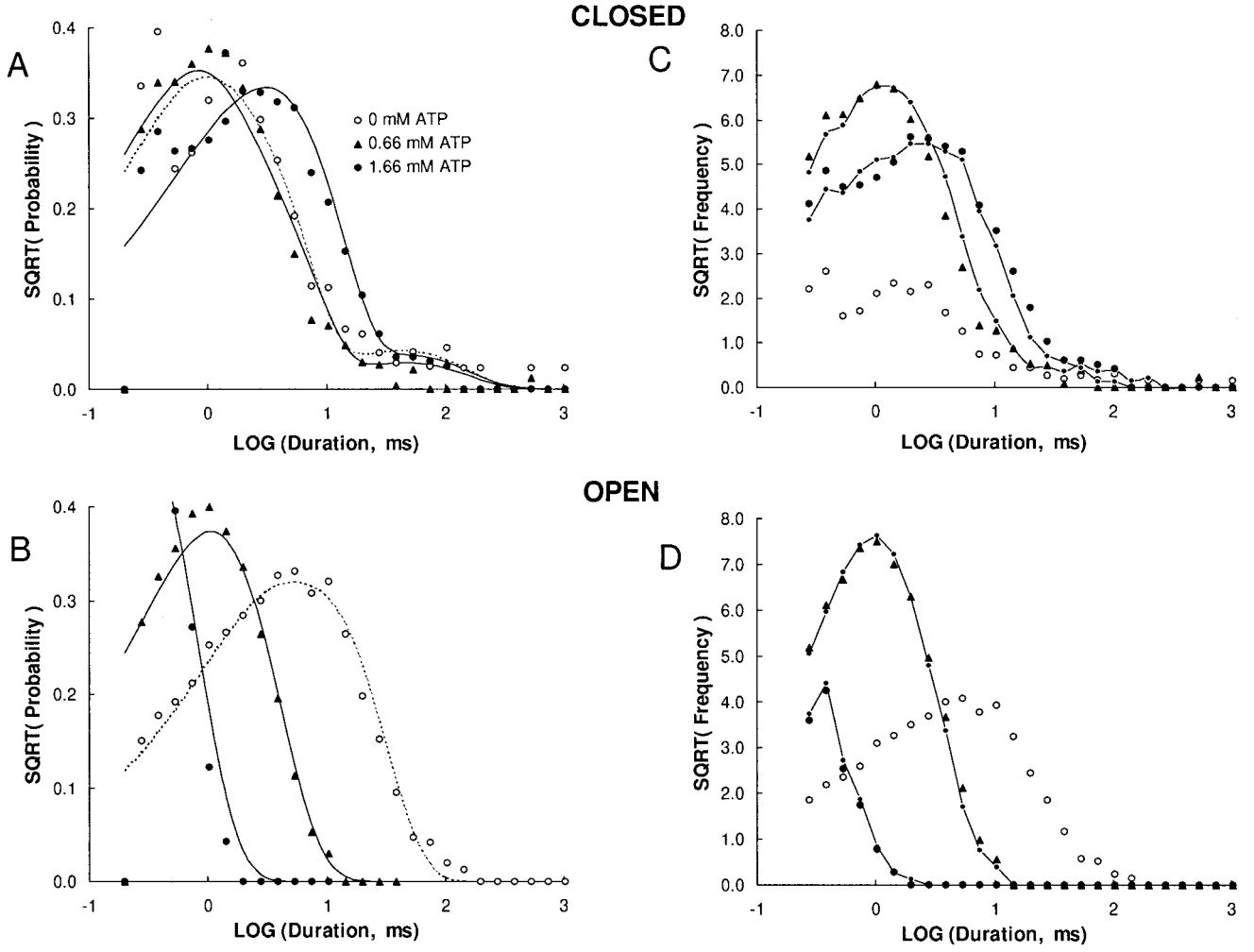

FIGURE 11 Dwell-time histograms of open and closed events for an SCl recorded at −40 mV with 0, 0.66, and 1.66 mM MgATP in the *cis* bath. In these experiments ATP inhibited channel activity (i.e., the mean current) by 33% and 80% at 0.66 and 1.66 mM, respectively. The data are plotted the same way as in Fig. 10. In *A* and *B* the distributions are shown as probability distributions that are compared to model fits (Scheme 1, *curved lines*). The effects of ATP on the channel open times are clearly seen in *B*. The dashed curve shows the fit to the control data, and the solid curves show the fits to the data obtained in 0.66 and 1.66 mM ATP. In *C* and *D* the dwell-time distributions are displayed in terms of event frequency (i.e., number of events per second of recording). In this format the effect of ATP on the closed time distribution is clearly seen. ATP enhances the frequency of closures with durations of ~1 ms. The small symbols connected by solid lines show the dwell time distributions from simulated records where ATP-induced closures have been inserted into the control record (open circles) in accordance with the model (see Results).

independently of its conducting state or exclusively in the channel open states. The ATP binding rate increased with increasing ATP concentration (Hill coefficient of ~2), and the ATP unbinding rate was independent of [ATP] (not shown). In the example shown in Fig. 11, the ATP binding rate increased by a factor of 6.3 between [ATP] values of 0.66 and 1.66 mM, corresponding to a Hill coefficient of 2.0. At the higher [ATP], the peak of the closed distribution moved to longer times. According to the model, this effect arises from a higher proportion of short openings at high [ATP], which go undetected by the recording and analysis procedures.

Voltage dependence

The effect of ATP on SCl channel dwell times was measured at −40, −60, and −80 mV. A shift in the membrane potential from −40 mV to −80 mV had the same effect on both open and closed dwell times as a threefold reduction in [ATP]. Thus varying the bilayer potential over this range had no effect on mean duration of ATP-induced closures, but had a large effect on the open dwell times. Fig. 12 shows the voltage dependence of the ATP binding and unbinding rate constants (see below). It can be seen from Fig. 12 that the voltage dependence of ATP inhibition is mediated primarily by the ATP binding rate.

Simulated ATP inhibition

Here several conclusions about ATP inhibition that were drawn from the analysis are tested by a simulation approach. Signal statistics of authentic recordings of ATP-inhibited channels were compared with those of simulated recordings

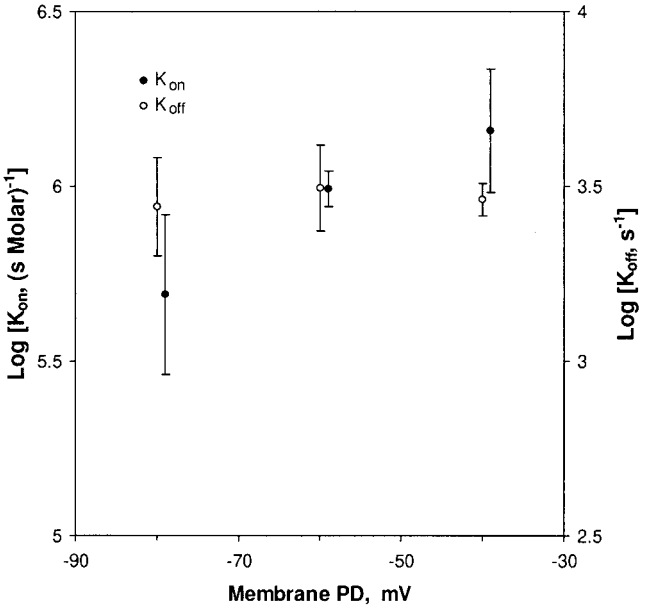

FIGURE 12 Voltage dependence of the ATP binding rates (K_{on}) and unbinding rate (K_{off}). The binding parameters were calculated from the transition probability matrix generated by the HMM algorithm. The data show that the voltage dependence of ATP inhibition is mainly due to the ATP binding step, because ATP unbinding is independent of voltage.

in which the underlying ATP inhibition mechanism is known. Recordings of SCl channels with simulated ATP inhibition were constructed and analyzed as described in Materials and Methods. The model for ATP inhibition was based on a mechanism in which the binding of ATP causes immediate closure of the channel and ATP dissociation opens the channel. The authentic and simulated recordings had identical filtering and background noise and were analyzed in the same way.

We tested the hypothesis that high conductance states of the SCl channel were equally inhibited by ATP, whereas the 20-pS substate was insensitive to ATP. As stated above, the effect of ATP on the higher conductance levels was analyzed in terms of model 1 with current levels at 0, −4, −6, and −8 pA. ATP inhibition was then mimicked by inserting closures into the authentic control data according to a model in which the probability of a simulated closure occurring at a given instant was independent of the conductance state of the channel. Table 1 compares the mean duration and probability of different current levels in simulated and authentic records at two ATP concentrations. The effects of ATP on the probabilities and dwell times of the higher conductance levels were accurately simulated by ATP binding independently of the channel conductance state. The effect of ATP on the 20-pS substate was analyzed in terms of model 2 with current levels at 0, −2, and −5 pA. As before, ATP inhibition was simulated by inserting closures into control recordings independently of the channel conductance state (SIM1). In addition, we simulated ATP inhibition where closures only occurred when the channel was in the highest (−5 pA) state (SIM 2). Table 2 compares the mean duration and probability of the −2-pA and −5-pA current levels from authentic and simulated records. SIM2 provided a closer match to the effects of ATP on substate probabilities and dwell times than SIM1. Hence the analysis of simulated inhibition supports a model in which ATP only affects the high conductance states of the channel.

We also used dwell-time distributions from the simulated records to verify the theoretical probability distribution functions from Scheme 1. The simulated recordings were generated by using the same model as that used to examine ATP inhibition of the higher conductance states in Table 1. The dwell-time histograms from simulated and authentic records are compared in Fig. 11, *C* and *D*. The model simulation is in agreement with the theoretical predictions. Both analytical approaches show that the model accounts for the effect of ATP on channel dwell times.

DISCUSSION

In this paper we describe in detail the inhibition by ATP of a small-conductance (75–105 pS) Ca^{2+}-activated anion channel (SCl) present in the SR of skeletal muscle. Hence, in addition to activation by Ca^{2+} and voltage, inhibition by ATP provides a further mechanism by which SCl channel activity can be regulated in vivo. ATP inhibition occurs independently of phosphorylation, because the blockade is reversible and is mimicked by the nonhydrolyzable ATP analog AMP-PNP. Inhibition by *cis* ATP only occurred when Cl^- flowed from the cytoplasmic to luminal bath. Conversely, inhibition by *trans* ATP was restricted to voltages where current flowed from the luminal to the cytoplasmic bath, suggesting that ATP can induce rectification from either side of the bilayer. Inhibition increased with adenine nucleotide concentration, and channels could be completely blocked at >3 mM. At −40 mV half-inhibition, K_I, of the maximum open probability was observed between 0.4 and 1 mM. Inhibition by *cis* ATP was also voltage dependent; inhibition was relieved with increasing negative potential. HMM analysis revealed that both ATP and AMP-PNP reduced mean channel open time without appreciably altering the maximum channel amplitude. Modeling of dwell-time distributions showed that ATP inhibition was mediated by a novel, single closed state of the channel. Comparative HMM analysis of simulated activity and authentic channel records indicated that ATP inhibits the substates within the high-conductance band of the channel with similar potency, whereas it does not inhibit the low-conductance substates.

Blocking potency of ATP complexes

The reduced potency of MgATP relative to Na_2ATP may be due to differences in the proportion of charged ATP species present. Because ATP has a higher affinity for Mg^{2+} compared to Na^+, there is a greater proportion of metal-bound ATP^{2-} relative to unbound ATP^{4-}, with Mg^{2+} than is the case for Na^+. For instance, the relative proportion of

ATP^{4-}, ATP^{3-}, and ATP^{2-} is ~26%, 40%, and 33%, respectively, with 1 mM Na_2ATP/1 mM Ca^{2+}, and ~17%, 26%, and 55%, respectively, with 1 mM MgATP/1 mM Ca^{2+}. Thus, with Mg^{2+} there is a clear shift to the ATP^{2-} complex. Furthermore, we have found that chelating free ATP^{4-}, by increasing total Ca^{2+} from 1 to 5 mM, reduces ATP inhibition (data not shown). Taken together, these observations suggest that the blocking potency of the ATP complexes increases with their negative charge. However, this interpretation is complicated by the fact that free [Ca^{2+}] was not held constant in these experiments (ATP chelates Ca^{2+} and Na_2ATP does so more effectively than MgATP). Thus an alternative explanation for the differences in the metal-ATP potencies, and the effects of raised [Ca^{2+}] is that the ATP-modified channel has an altered Ca^{2+} dependency that requires higher [Ca^{2+}] than normal (~100 μM) for maximum activation. Hence the channel would deactivate as the free [Ca^{2+}] decreases within the range 0.5–1 mM because of the chelating effects of ATP addition.

Two pieces of evidence show that it is unlikely that ATP inhibition is merely a manifestation of Ca^{2+} deactivation. First, whereas the proportions of ATP complexes with 1 mM Na_2ATP and MgATP are very different (as outlined above), free [Ca^{2+}] is similar in the two cases (0.64 mM and 0.72 mM), and therefore the different potencies of the ATP salts do not appear to correlate with [Ca^{2+}]. Second, the properties of ATP inhibition are distinctly different from those of Ca^{2+} deactivation. Our results showed that the addition of up to 9 mM *cis* ATP (which reduced free [Ca^{2+}] from 1 mM to 0.35 mM) did not inhibit channel activity when Cl^- flowed from the luminal to cytoplasmic baths. Thus deactivation does not occur in the range of free [Ca^{2+}] produced by ATP chelation.

Comparison with previous work

Several of our results confirm the findings of a recent study of ATP inhibition of the SCl channel (Kourie, 1997). Kourie reported a phosphorylation-independent block by *cis* or *trans* ATP, that half-maximum block by *cis* ATP in one channel occurred at ~0.3–0.5 mM (similar to the K_I values we report for Na_2ATP and Li_2AMP-PNP) and that inhibition correlated with the charge of the adenine nucleotide species. Kourie also showed that ATP inhibition is mediated by a reduction in channel open time. The relative insensitivity of SCl substates to inhibition by ATP can also be seen in single-channel recordings (Fig. 4; Kourie, 1997), although he does not comment on this result. The present study extends the previous work by presenting a detailed investigation of the effects of membrane voltage, current direction, SCl conductance state, and ATP net charge on the kinetics of ATP inhibition. We also address effects of ATP on burst durations.

There are a number of differences in our findings and those of Kourie (1997). The major difference is in the voltage dependence of *cis* ATP inhibition. We found that channels were maximally inhibited by ATP at ~0 mV, whereas the Kourie study found only minimal inhibition at ~0 mV and no apparent voltage dependence of ATP inhibition. The reason for the discrepancy is not clear, but may have resulted from the different voltage protocols used to record SCl channel activity. In the Kourie study, non-steady-state SCl activity was measured in response to voltage steps from a holding potential of +60 mV to a range of potentials between +50 and −70 mV. In this study ATP inhibition was measured under steady-state conditions. Under non-steady-state conditions the ATP effect could be a combination of ATP inhibition plus ATP-dependent changes in SCl channel activation and inactivation rates.

Kourie (1997) reported that ATP causes a reduction in maximum current amplitude, whereas we find that SCl conductance levels are only marginally affected by ATP. Kourie's result is due to both the effect of filtering on the reduced channel open times and the use of all-points amplitude histograms to measure channel conductance. We found that the peaks in all-points amplitude histograms were an unreliable measure of conductance in the SCl channel with many substates. In addition, Kourie (1997) reported that channels are similarly inhibited by MgATP and Na_2ATP and that the addition of 5–10 mM Ca^{2+} had no effect on ATP inhibition, i.e., chelation of free ATP^{4-} had no effect on blocking potency. However, we find that the Mg^{2+} salt of ATP is less effective than Na_2ATP, and that addition of >5 mM Ca^{2+} partly alleviates ATP block. Our data suggest that inhibition by the different ATP complexes depends on their net charge, and this finding is consistent with the charge dependence of adenine nucleotide block seen by Kourie (1997), i.e., $ATP^{4-} > ADP^{2-} > AMP$.

A blocking mechanism for ATP inhibition

Several lines of evidence suggest that ATP inhibits SCl channel activity by lodging within the ion conduction pathway and blocking the pore. The key observation supporting this conclusion is that the potency of block by *cis* ATP is strongly dependent on the direction of the Cl^- flux in the pore (see Figs. 6–8). This indicates that the *cis* ATP binding site is directly accessible to Cl^- in the *trans* bath when the net Cl^- flux is from *trans* to *cis*. Further evidence in support of an ATP blocking mechanism is that inhibition by ATP depends on the membrane potential and may also depend on the net charge of the blocking species (see above), indicating that the nucleotide binding region lies within the membrane electric field. These results, taken together with the observation that HPO_4^{2-} (10 mM) does not inhibit activity and is permeable through the SCl channel (see below), suggest that block by adenine nucleotides is due to their increased charge or size.

Although the interpretation of the Hill coefficient for the dose response of nucleotide inhibition may be limited (as described above), it nonetheless suggests that channel block results from the binding of more than one ATP molecule.

Thus ATP block may be a multiion process that cannot be described solely by the interaction of a single ion with the channel protein (i.e., a single-ion mechanism). Inhibition by cytoplasmic ATP at negative potentials had a voltage dependence opposite that expected by the Woodhull model (Woodhull, 1973), in which a negative potential difference drives ATP onto the channel protein and inhibits the channel, and positive potentials relieve the block. The reason for the anomalous voltage dependence seen here is not known. In other studies of ion block, anomalous voltage dependencies were attributed to block-permeation mechanisms in which association and subsequent dissociation from the blocking site allow the blocking ion to traverse the membrane (Laver, 1992; Neyton and Miller, 1988). In these studies ion block was characterized by voltage-dependent closed dwell times, whereas the voltage dependence of ATP block seen here was mediated by voltage-dependent open dwell times. However, on this basis a block-permeation mechanism cannot be ruled out, because a similar mechanism involving two ATP molecules can explain the anomalous voltage dependence of open dwell times. Furthermore, several mechanisms have been proposed in which several ions interact within the conducting pathway to produce block with an anomalous voltage dependence (multiion mechanisms, e.g., Cecchi et al., 1987; Eisenman et al., 1986). The data presented here are insufficient to allow us to distinguish between alternative multiion models.

The potency of ATP block depends on the conducting state of the pore. Pore conformations that produce low conductance states of the SCl channel have a relatively low affinity for adenine nucleotides. We are unable to tell whether or not ATP can bind to the channel in its closed state. If ATP does inhibit via an open channel block mechanism, then this would be consistent with mechanisms proposed for ATP inhibition of an anion channel from human platelet surface membrane (Manning and Williams, 1989) and Cl^- channels from outer nuclei membrane (Rousseau et al., 1996; Tabares et al., 1991).

It remains possible that ATP inhibition partly involves allosteric effects due to binding to a specific adenine nucleotide binding site inside or outside the pore. Whereas a number of Cl^- channels are known to be activated by ATP binding (for example, a volume-regulated Cl^- channel in epithelial cells is directly activated by binding alone (Oiki et al., 1994) and the cystic fibrosis transport regulator (CFTR) is activated by concomitant nucleotide binding and hydrolysis (Anderson and Welsh, 1992)), there are few reports of an allosteric-mediated inhibition of Cl^- channel activity; in fact, we are aware of only a single report, on a synaptosomal anion channel (Yuto et al., 1997).

The observations that SCl channels are inhibited by a variety of nucleotides and polyanions, including GTP (Kourie, 1997), IP_3, IP_4, heparin, and vanadate (Kourie et al., 1997), indicates that ATP inhibition is independent of the nucleotide base and suggests that these compounds have a similar blocking action. Interestingly, in the latter study the authors propose that inositol polyphosphate inhibition occurs at a polyanion site located on the cytoplasmic portion of the channel, and not by an open channel block mechanism. They conclude this based on the failure of IP_3 to block from the *trans* side of the bilayer. However, they did not investigate any voltage dependence of block by inositol polyphosphates and only measured effects of *trans* ATP at a single voltage (-40 mV), the potential at which we show relief of ATP block. Thus it is possible that they failed to observe inhibition at this potential because of the same voltage-dependence/rectification we report here for adenine nucleotides.

Physiological significance

We have previously proposed that the SCl channel may contribute to a Cl^- countercurrent necessary to balance electrogenic Ca^{2+} uptake into the SR (Kourie et al., 1996a). Such a role is analogous to anion channels, which enhance Ca^{2+} uptake in pancreatic ER. In addition, it has been suggested that SCl channel block by certain polyanions including, IP_3 and IP_4, may reduce Ca^{2+} uptake and increase myoplasmic [Ca^{2+}] (Kourie et al., 1997). A major difficulty in accepting a Cl^- countercurrent role for the SCl channel is the coexistence in the SR of a very active, large-conductance Cl^- channel; the conductance through this large channel would overwhelm that of SCl channels. Moreover, the ATP inhibition described here is unlikely to allow the SCl channel to conduct a countercurrent in vivo to balance Ca^{2+} uptake, and raises the question of whether the SCl channel functions as a chloride channel at all. Half-maximum inhibition by *cis* MgATP was ~1 mM at -40 mV (and ~100 μM at 0 mV), and channel activity was nearly completely blocked at ~3 mM. Moreover, the potency of ATP inhibition could be far greater in vivo, where [Cl^-] is 20-fold lower (~7 mM) than in the bilayer experiments, because we found that high [Cl^-] tended to alleviate ATP inhibition (data not shown). Because [MgATP] is ~5–7 mM under normal physiological conditions, one would expect that cytoplasmic to luminal current through SCl channels would be strongly inhibited, even under conditions of extreme muscle fatigue, where [ATP] is decreased. If the SCl channel is involved in charge balance at all, then it would be restricted to balancing Ca^{2+} release and not uptake.

Alternatively, small-subconductance states (~20 pS) were relatively immune to ATP inhibition over the range 1–2 mM, and may therefore have an important physiological role. In addition, it is possible that ATP inhibition may be modified by other cytosolic factors, as has been proposed for ATP inhibition of K_{ATP} channels. For example, reducing pH from 7.2 to 6.3 decreases the ATP affinity of K_{ATP} channels by ~15-fold and is consistent with competition between proton and ATP binding (Standen, 1992).

It is also possible that protons or other polyanions compete with ATP and Cl^- for SCl channels. One candidate is HPO_4^{2-}, which, as we report here, does not block channel

activity at up to 10 mM concentrations and is itself permeable through the SCl channel (D. Laver, unpublished observations). During exercise, myoplasmic HPO_4^{2-} can rise from ~1–5 to 30 mM, and HPO_4^{2-} accumulates in the lumen of the SR (Fruen et al., 1994; Fryer et al., 1997). The SR membrane is permeable to HPO_4^{2-} (see Fryer et al., 1997), and HPO_4^{2-} is commonly used to facilitate Ca^{2+} loading of the SR and SR vesicles. Two HPO_4^{2-} transport mechanisms have been identified in the SR: 1) active uptake powered by ATP hydrolysis (Stefanova et al., 1991), and 2) passive efflux (Posterino and Fryer, 1997). Therefore it is quite possible that the SCl channel has a physiological role in HPO_4^{2-} efflux, and this would be consistent with ATP-induced rectification. It is then also relevant that the channel has been identified in skeletal muscle, where HPO_4^{2-} levels fluctuate enormously, but not in cardiac SR, where HPO_4^{2-} levels are uniformly low (Fruen et al., 1994).

Finally, it is possible that the SCl channel is itself permeable to ATP. This possibility is based on the voltage-dependent relief of ATP inhibition observed at negative potentials. One obvious explanation for this phenomenon is a block-permeation mechanism (described above) in which ATP is pushed through the channel pore with increased negative potential, thereby diminishing block of Cl^- current. As explained above, our results do not give an unequivocal answer to the possibility of a block-permeation mechanism, and it remains possible that the SCl channel does contribute to ATP transport. On this note, the VDAC channel, traditionally considered a mitochondrial channel, has been detected in SR (Junankar et al., 1995) and has been implicated in ATP transport into the SR lumen (Shoshan-Barmatz et al., 1996). Shoshan-Barmatz et al. reported that inhibiting VDAC reduced phosphorylation of intraluminal proteins. Therefore, it would be interesting to test whether inhibition of SCl channels can also affect the degree of SR protein phosphorylation.

In conclusion, our results show that ATP produces a luminal to cytoplasmic rectification of SCl channels and that ATP inhibition is dependent on both the membrane voltage and the conductance level of the channel. These findings suggest that the SCl channel is unlikely to provide a countercurrent to Ca^{2+} uptake and point to the channel having a role in the transport of other anions across the SR.

We thank Drs. Pauline Junankar and Angela Dulhunty for lively discussion and critical comments on the manuscript. We also thank Suzy Pace and Joan Stivala for preparing the SR vesicles.

REFERENCES

Ahern, G. P., P. R. Junankar, and A. F. Dulhunty. 1994. Single channel activity of the ryanodine receptor calcium release channel is modulated by FK-506. *FEBS Lett.* 352:369–374.

Ahern, G. P., P. R. Junankar, and A. F. Dulhunty. 1997. Subconductance states in single-channel activity of skeletal muscle ryanodine receptors after removal of FKBP12. *Biophys. J.* 72:146–162.

Anderson, M. P., and M. J. Welsh. 1992. Regulation by ATP and ADP of CFTR chloride channels that contain mutant nucleotide-binding. *Science.* 257:1701–1704.

Blatz, A. L., and K. L. Magleby. 1986. Correcting single channel data for missed events. *Biophys. J.* 49:967–980.

Brooks, S. P., and K. B. Storey. 1992. Bound and determined: a computer program for making buffers of defined ion concentrations. *Anal. Biochem.* 201:119–126.

Cecchi, X., D. Wolff, O. Alvarez, and R. Latorre. 1987. Mechanisms of Cs^+ blockade in a Ca^{2+}-activated K^+ channel from smooth muscle. *Biophys. J.* 52:707–716.

Chung, S. H., and R. A. Kennedy. 1996. Coupled Markov chain model: characterization of membrane channel currents with multiple conductance sublevels as partially coupled elementary pores. *Math. Biosci.* 133:111–137.

Chung, S. H., V. Krishnamurthy, and J. B. Moore. 1991. Adaptive processing techniques based on hidden Markov models for characterizing very small channel currents buried in noise and deterministic interferences. *Philos. Trans. R. Soc. Lond. Biol.* 334:357–384.

Chung, S. H., J. B. Moore, L. G. Xia, L. S. Premkumar, and P. W. Gage. 1990. Characterization of single channel currents using digital signal processing techniques based on hidden Markov models. *Philos. Trans. R. Soc. Lond. Biol.* 329:265–285.

Colquhoun, D., and A. G. Hawkes. 1981. On the stochastic properties of single ion channels. *Proc. R. Soc. Lond. Biol.* 211:205–35.

Coronado, R., J. Morrissette, M. Sukhareva, and D. M. Vaughan. 1994. Structure and function of ryanodine receptors. *Am. J. Physiol.* 266: C1485–C1504.

Coronado, R., R. L. Rosenberg, and C. Miller. 1980. Ionic selectivity, saturation, and block in a K^+-selective channel from sarcoplasmic reticulum. *J. Gen. Physiol.* 76:425–446.

Eisenman, G., R. Latorre, and C. Miller. 1986. Multi-ion conduction and selectivity in the high-conductance Ca^{++}-activated K^+ channel from skeletal muscle. *Biophys. J.* 50:1025–1034.

Fink, R. H., and C. Veigel. 1996. Calcium uptake and release modulated by counter-ion conductances in the sarcoplasmic reticulum of skeletal muscle. *Acta Physiol. Scand.* 156:387–396.

Fruen, B. R., P. K. Kane, J. R. Mickelson, and C. F. Louis. 1996. Chloride-dependent sarcoplasmic reticulum Ca^{2+} release correlates with increased Ca^{2+} activation of ryanodine receptors. *Biophys. J.* 71: 2522–2530.

Fruen, B. R., J. R. Mickelson, N. H. Shomer, T. J. Roghair, and C. F. Louis. 1994. Regulation of the sarcoplasmic reticulum ryanodine receptor by inorganic phosphate. *J Biol. Chem.* 269:192–198.

Fryer, M. W., J. M. West, and D. G. Stephenson. 1997. Phosphate transport into the sarcoplasmic reticulum of skinned fibres from rat skeletal muscle. *J. Muscle Res. Cell Motil.* 18:161–167.

Hamilton, S. L., R. M. Alvarez, M. Fill, M. J. Hawkes, K. L. Brush, W. P. Schilling, and E. Stefani. 1989. [^{3}H]PN200-110 and [^{3}H]ryanodine binding and reconstitution of ion channel activity with skeletal muscle membranes. *Anal Biochem.* 183:31–41.

Ikemoto, N., M. Yano, R. el-Hayek, B. Antoniu, and M. Morii. 1994. Chemical depolarization-induced SR calcium release in triads isolated from rabbit skeletal muscle. *Biochemistry.* 33:10961–10968.

Junankar, P. R., A. F. Dulhunty, S. M. Curtis, S. M. Pace, and F. P. Thinnes. 1995. Porin-type 1 proteins in sarcoplasmic reticulum and plasmalemma of striated muscle fibres. *J. Muscle Res. Cell Motil.* 16:595–610.

Kemmer, T. P., E. Bayerdorffer, H. Will, and I. Schulz. 1987. Anion dependence of Ca^{2+} transport and (Ca^{2+} + K^+)-stimulated Mg^{2+}-dependent transport ATPase in rat pancreatic endoplasmic reticulum. *J. Biol. Chem.* 262:13758–13764.

Kourie, J. I. 1997. ATP-sensitive voltage- and calcium-dependent chloride channels in sarcoplasmic reticulum vesicles from rabbit skeletal muscle. *J. Membr. Biol.* 157:39–51.

Kourie, J. I., P. S. Foster, and A. F. Dulhunty. 1997. Inositol polyphosphates modify the kinetics of a small chloride channel in skeletal muscle sarcoplasmic reticulum. *J. Membr. Biol.* 157:147–158.

Kourie, J. I., D. R. Laver, G. P. Ahern, and A. F. Dulhunty. 1996a. A calcium-activated chloride channel in sarcoplasmic reticulum vesicles from rabbit skeletal muscle. *Am. J. Physiol.* 270:C1675–C1686.

Kourie, J. I., D. R. Laver, P. R. Junankar, P. W. Gage, and A. F. Dulhunty. 1996b. Characteristics of two types of chloride channel in sarcoplasmic reticulum vesicles from rabbit skeletal muscle. *Biophys. J.* 70:202–221.

Laver, D. R. 1992. Divalent cation block and competition between divalent and monovalent cations in the large-conductance K^+ channel from *Chara australis. J. Gen. Physiol.* 100:269–300.

Laver, D. R., L. D. Roden, G. P. Ahern, K. R. Eager, P. R. Junankar, and A. F. Dulhunty. 1995. Cytoplasmic Ca^{2+} inhibits the ryanodine receptor from cardiac muscle. *J. Membr. Biol.* 147:7–22.

Manning, S. D., and A. J. Williams. 1989. Conduction and blocking properties of a predominantly anion-selective channel from human platelet surface membrane reconstituted into planar phospholipid bilayers. *J. Membr. Biol.* 109:113–122.

Marks, P. W., and F. R. Maxfield. 1991. Preparation of solutions with free calcium concentration in the nanomolar range using 1,2-bis(*o*-aminophenoxy)ethane-*N*,*N*,*N*′,*N*′-tetraacetic acid. *Anal. Biochem.* 193: 61–71.

Meissner, G., E. Rios, A. Tripathy, and D. A. Pasek. 1997. Regulation of skeletal muscle Ca^{2+} release channel (ryanodine receptor) by Ca^{2+} and monovalent cations and anions. *J. Biol. Chem.* 272:1628–1638.

Miller, C., and E. Racker. 1976. Ca^{++}-induced fusion of fragmented sarcoplasmic reticulum with artificial planar bilayers. *Cell.* 9:283–300.

Neyton, J., and C. Miller. 1988. Potassium blocks barium permeation through a calcium-activated potassium channel. *J. Gen. Physiol.* 92: 549–567.

Oiki, S., M. Kubo, and Y. Okada. 1994. Mg^{2+} and ATP-dependence of volume-sensitive Cl^- channels in human epithelial cells. *Jpn. J. Physiol.* 44(Suppl. 2):S77–S79.

Patlak, J. B. 1988. Sodium channel subconductance levels measured with a new variance-mean analysis. *J. Gen. Physiol.* 92:413–430.

Posterino, G. S., and M. W. Fryer. 1997. Time course of inorganic phosphate (P_i) removal from the sarcoplasmic reticulum of rat fast-twitch skeletal muscle. *Proc. Aust. Physiol. Pharmacol. Soc.* 28:85P.

Rostovtseva, T., and M. Colombini. 1997. VDAC channels mediate and gate the flow of ATP: implications for the regulation of mitochondrial function. *Biophys. J.* 72:1954–1962.

Rousseau, E., C. Michaud, D. Lefebvre, S. Proteau, and A. Decrouy. 1996. Reconstitution of ionic channels from inner and outer membranes of mammalian cardiac nuclei. *Biophys. J.* 70:703–714.

Ruegg, J. C. 1988. Calcium in Muscle Activation. Springer Verlag, New York.

Saito, A., S. Seiler, A. Chu, and S. Fleischer. 1984. Preparation and morphology of sarcoplasmic reticulum terminal cisternae from rabbit skeletal muscle. *J. Cell Biol.* 99:875–885.

Shoshan-Barmatz, V., N. Hadad, W. Feng, I. Shafir, I. Orr, M. Varsanyi, and L. M. Heilmeyer. 1996. VDAC/porin is present in sarcoplasmic reticulum from skeletal muscle. *FEBS Lett.* 386:205–210.

Sigworth, F. J., and S. M. Sine. 1987. Data transformations for improved display and fitting of single-channel dwell time histograms. *Biophys. J.* 52:1047–1054.

Somlyo, A. V., H. G. Gonzalez-Serratos, H. Shuman, G. McClellan, and A. P. Somlyo. 1981. Calcium release and ionic changes in the sarcoplasmic reticulum of tetanized muscle: an electron-probe study. *J. Cell Biol.* 90:577–594.

Standen, N. B. 1992. The G. L. Brown Lecture. Potassium channels, metabolism and muscle. *Exp. Physiol.* 77:1–25.

Stefanova, H. I., J. M. East, and A. G. Lee. 1991. Covalent and non-covalent inhibitors of the phosphate transporter of sarcoplasmic reticulum. *Biochim. Biophys. Acta.* 1064:321–328.

Sukhareva, M., J. Morrissette, and R. Coronado. 1994. Mechanism of chloride-dependent release of Ca^{2+} in the sarcoplasmic reticulum of rabbit skeletal muscle. *Biophys. J.* 67:751–765.

Tabares, L., M. Mazzanti, and D. E. Clapham. 1991. Chloride channels in the nuclear membrane. *J. Membr. Biol.* 123:49–54.

Tanifuji, M., M. Sokabe, and M. Kasai. 1987. An anion channel of sarcoplasmic reticulum incorporated into planar lipid bilayers: single-channel behavior and conductance properties. *J. Membr. Biol.* 99: 103–111.

Woodhull, A. M. 1973. Ionic blockage of sodium channels in nerve. *J. Gen. Physiol.* 61:687–708.

Yu, X., L. Hao, and G. Inesi. 1994. A pK change of acidic residues contributes to cation countertransport in the Ca-ATPase of sarcoplasmic reticulum. Role of H^+ in $Ca(^{2+})$-ATPase countertransport. *J. Biol. Chem.* 269:16656–16661.

Yuto, J., T. Ide, and M. Kasai. 1997. ATP-sensitive anion channel from rat brain synaptosomal membranes incorporated into planar lipid bilayers. *Biophys. J.* 72:720–727.

Zimniak, P., and E. Racker. 1978. Electrogenicity of Ca^{2+} transport catalyzed by the Ca^{2+}-ATPase from sarcoplasmic reticulum. *J. Biol. Chem.* 253:4631–4637.